Opto-Electronic Science

Supplementary information

2022, Vol. 1, No. 3

DOI: 10.29026/oes.2022.210006

Single-shot mid-infrared incoherent holography using Lucy-Richardson-Rosen algorithm

Vijayakumar Anand[1, 2*], Molong Han[1], Jovan Maksimovic[1], Soon Hock Ng[1], Tomas Katkus[1], Annaleise Klein[3], Keith Bambery[3], Mark J. Tobin[3], Jitraporn Vongsvivut[3*] and Saulius Juodkazis[1, 4*]

[1]Optical Optical Sciences Center and ARC Training Centre in Surface Engineering for Advanced Materials (SEAM), School of Science, Computing and Engineering Technologies, Optical Sciences Center, Swinburne University of Technology, Hawthorn, Melbourne, Victoria 3122, Australia; [2]Institute of Physics, University of Tartu, 50411 Tartu, Estonia; [3]Infrared Microspectro scopy (IRM) Beamline, ANSTO – Australian Synchrotron, Clayton, Victoria 3168, Australia; [4]Tokyo Tech World Research Hub Initiative (WRHI), School of Materials and Chemical Technology, Tokyo Institute of Technology, 2-12-1, Ookayama, Meguro-ku, Tokyo 152-8550, Japan.

*Correspondence: V Anand, E-mail: vanand@swin.edu.au; J Vongsvivut, E-mail: jitrapov@ansto.gov.au;
S Juodkazis, E-mail: sjuodkazis@swin.edu.au

This file includes:

Supplementary information for this paper is available at https://doi.org/10.29026/oes.2022.210006

Section 1: Theoretical analysis

The phase of a Cassegrain objective lens (COL) is approximated by an annular diffractive lens or diffractive equivalent COL (DE-COL) at a single wavelength λ. In addition to that COL is mounted with a cross shaped block as shown in Fig. S1(a), which modulates the transmittance. The phase image of the COL can be approximated as shown in Fig. S1(b). A simplified optical configuration of imaging is shown in Fig. S1(c). The complex amplitude introduced by the COL can be approximated (Fresnel approximation)[1] as:

$$C_{\text{DE-COL}} = M_1 M_2 \exp\left(-\mathrm{j}\frac{\pi r^2}{\lambda f}\right), R_1 \le r < R_2 ,$$

where M_1 is the transmittance function of the cross shaped block, $M_2 = \begin{cases} 0, r < R_1 \\ 1, R_1 \le r < R_2 \end{cases}$; R_1 and R_2 are the inner and outer radii of the annulus and f is the focal length, which is designed for finite conjugate mode given as $f = \frac{1}{u'} + \frac{1}{v}$.

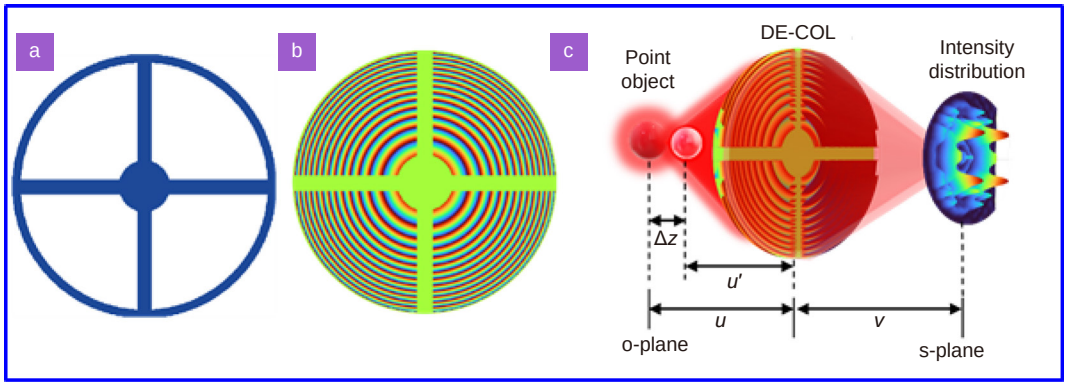

Fig. S1 | (**a**) Mount of COL. (**b**) Phase image of DE-COL. (**c**) Simplified optical configuration for imaging using DE-COL.

The theoretical analysis is from the object plane (o-plane) located at u' from DE-COL to the sensor plane (s-plane) at v from DE-COL. The proposed system is a spatially incoherent imaging system. A self-luminous point object located at $(\overline{r_o}, u)$ emits light, which reaches the DE-COL with an intensity I_o where $u = u' + \Delta z$ and Δz is the axial shift error. The complex amplitude reaching the DE-COL plane can be given as $C_1\sqrt{I_o}L(\overline{r_o}/u)Q(1/u)$, where C_1 is a complex constant, $\overline{r_o} = (x_o, y_o)$, $L(\overline{o}/u) = \exp[\mathrm{j}2\pi(o_x x + o_y y)/(\lambda u)]$ and $Q(1/u) = \exp[\mathrm{j}\pi(r^2)/(\lambda u)]$ are the linear and quadratic phase factors. The complex amplitude after the DE-COL is given as $C_1\sqrt{I_o}L(\overline{r_o}/u)Q(1/u)C_{\text{DE-COL}}$. As COL does not have notable spectral aberrations, the wavelength dependent analysis is not considered. The intensity pattern obtained at the sensor plane located at v from the DE-COL is given as:

$$I_{\text{PSF}}(\overline{r_s}; \overline{r_o}, u) = \left| C_1\sqrt{I_o}L\left(\frac{\overline{r_o}}{u}\right) Q\left(\frac{1}{u}\right) C_{\text{DE-COL}} \otimes Q\left(\frac{1}{v}\right)\right|^2 , \tag{S1}$$

where '$\otimes$' is the 2D convolutional operator. The above equation can be expressed as:

$$I_{\text{PSF}}(\overline{r_s}; \overline{r_o}, u) = I_{\text{PSF}}\left(\overline{r_s} - \frac{v}{u}\overline{r_o}; 0, u\right) . \tag{S2}$$

A two-dimensional chemical object p located in the object plane o consisting of M points is given as:

$$p(\overline{r_o}) = \sum_{i=1}^{M} t_i \delta(r - r_i) , \tag{S3}$$

where t_i is the transmitted intensity. Every δ point generates an intensity pattern given as $I_{\text{PSF}}(\overline{r_s}; \overline{r_o}, u)$ with a shift from the optical axis depending upon the acquired linear phase. The intensity distribution obtained for the object is given as:

$$I_p(\overline{r_s}, u) = \sum_{i=1}^{M} t_i I_{\text{PSF}}\left(\overline{r_s} - \frac{v}{u}\overline{r_{o,i}}; 0, u\right) , \tag{S4}$$

where the transverse magnification $M_T = (v/u)$. There are two cases: $\Delta z = 0$ and $\Delta z \neq 0$. When $\Delta z = 0$, direct imaging condition is satisfied and $I_p(\overline{r_s}, u) = p\left(\frac{\overline{r_o}}{M_T}\right)$, which is a magnified version of the object the with minimum feature given

by $1.22\lambda v/D$ on the camera, where D is the diameter of the DE-COL. When $\Delta z \neq 0$, $I_p\left(\overline{r_s}, u\right) = p'\left(\frac{\overline{r_o}}{M_T}\right)$, which is a distorted image of the object formed by the convolution of distorted PSF with p. As it is seen here, unlike random field based sharp autocorrelation and low cross-correlation along depth (SALCAD), deterministic SALCADs can have dual mode, i.e., both direct imaging and indirect imaging can co-exist. In any thick sample, the planes within the depth of focus $\pm 2(u')^2\lambda/D^2$ can be observed without the need for any reconstruction, which is different from SALCADs based on random fields.

Section 2: Simulation of focal characteristics of DE-COL

A simulative study of the DE-COL was carried out and the images of the intensity distributions obtained in the sensor plane for different values of shift errors for a regular diffractive lens are shown in Fig. S2. It demonstrates that even though the recorded intensity distribution is not a point, the autocorrelation is sharp which is the resolving power in indirect imaging mode. The cross-correlation for all images was carried out with respect to the reference image Δz (ref), except for the two planes that the cross-correlation is lower for other planes.

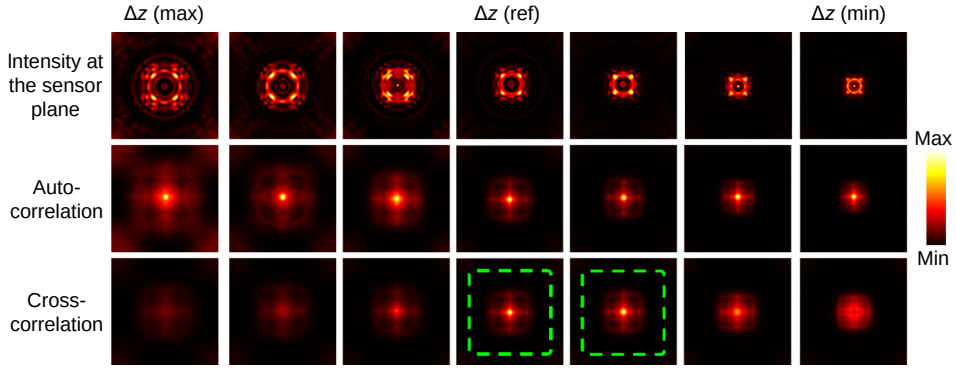

Fig. S2 | Simulated intensity distributions, autocorrelation and cross-correlation for DE-COL observed at different values of Δz. The sharpest cross-correlations are indicated in the green squares.

Section 3: Lucy-Richardson-Rosen algorithm

Lucy-Richardson-Rosen algorithm (LRRA) has been built using the well-known Lucy-Richardson algorithm (LRA)[2,3] and the recently developed non-linear reconstruction (NLR) method of Rosen[4]. The approaches for reconstruction by LRRA and NLR are quite different from one another. If I_{PSF} and p are the point spread function and object function respectively, then the object intensity distribution for a linear optical system in intensity is given as $I_p = I_{\mathrm{PSF}}p$. However, in practical cases, the expression is not always true due to noise σ. The noise σ can be signal dependent Poisson noise or additive noise or both. The correct expression for the intensity distribution for an object is given as $I_p = I_{\mathrm{PSF}}p + \sigma$. For this reason, the correlation by the matched filter, which is exactly the opposite operation of convolution does not yield the optimal solution[5].

The reconstructed image by NLR is given as $I_R = \left|\mathcal{F}^{-1}\left\{\left|\widetilde{I}_{\mathrm{PSF}}\right|^{\alpha}\exp\left[\mathrm{iarg}\left(\widetilde{I}_{\mathrm{PSF}}\right)\right]\left|\widetilde{I}_p\right|^{\beta}\exp\left[-\mathrm{iarg}\left(\widetilde{I}_p\right)\right]\right\}\right|$ and α and β are tuned between −1 and 1, to obtain the minimum entropy given as $S(p,q) = -\sum\sum\varphi(m,n)\log\left[\varphi(m,n)\right]$, where $\varphi(m,n) = |C(m,n)| / \sum_M\sum_N |C(m,n)|$, (m,n) are the indices of the correlation matrix, and $C(m,n)$ is the correlation distribution, and $\widetilde{I}_{\mathrm{PSF}}$ and $\widetilde{I}_p$ are the Fourier transforms of I_{PSF} and I_p, respectively. The magnitude of the spectrum of I_{PSF} and I_p are tuned before multiplication and inverse Fourier transform until the background noise is minimized. The solution obtained from NLR is more accurate than matched filter and phase-only filters. In the past studies, NLR has been applied only to random fields.

The LRA approach is iterative, where the $(n+1)^{\mathrm{th}}$ reconstructed image is given as $I_R^{n+1} = I_R^n\left\{\frac{I_p}{I_R^n \otimes I_{\mathrm{PSF}}} \otimes I_{\mathrm{PSF}}{}'\right\}$, where $I_{\mathrm{PSF}}{}'$ refers to the complex conjugate of I_{PSF} and the loop is iterated until an optimal reconstruction is obtained. In fact, the LRA has been widely used for astronomical imaging, where the recorded image is distorted or blurred. In many cases, the blurred image is not very different from the original image unlike scattering based images, where the object

information is converted into speckles. For this reason, LRA's initial guess is often the recorded image itself and the final solution is a maximum-likelihood solution. As seen in the above equation, there is a forward convolution $I_R^n \otimes I_{\mathrm{PSF}}$ and the ratio between this and I_p is correlated with I_{PSF}, which is replaced by the NLR and yields a better estimation. Consequently, the process achieves a rapid convergence.

Here, a test object "Lucy Richardson Rosen" has been selected as shown in Fig. S3(a). The image of the deterministic PSF generated by COL is shown in Fig. S3(b). The distorted image of the test object is shown in Fig. S3(c). The reconstruction results using LRA (iterations = 500), NLR ($\alpha = 0$, $\beta = 0.5$) and LRRA ($\alpha = 0$, $\beta = 0.6$, iterations = 10) are shown in Fig. S3(d–f), respectively. The LRRA is not only more than 50 times faster than LRA, but also a significantly better estimate than both LRA and NLR.

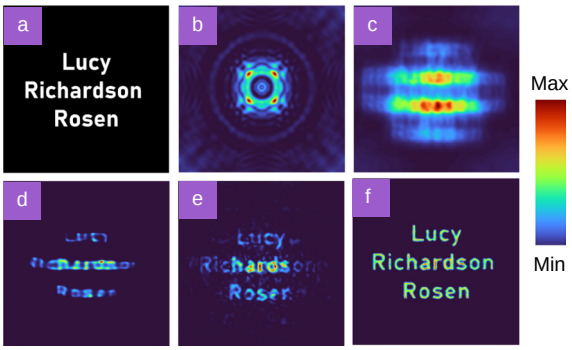

Fig. S3 | (**a**) Test object. (**b**) PSF of COL. (**c**) Distorted image of the object. Reconstruction results using (**d**) LRA (500 iterations), (**e**) NLR ($\alpha = 0$, $\beta = 0.5$), and (**f**) LRRA ($\alpha = 0$, $\beta = 0.6$, iterations = 10).

Section 4: Synthesis of PSFs from recorded PSF

In most of the studies of scattering-based 3D imagers, it was necessary to record the PSFs at all possible axial locations mainly due to the fact that they are not deterministic[6,7]. Some studies had utilized the linear region of propagation to apply the scaling factor to synthesize the PSFs from one or two recorded PSFs[8,9]. However, this linear region is quite short. The above disadvantage does not exist with deterministic fields, where the modulation function can be generated using one or two recorded PSFs based on phase-retrieval algorithms. The schematic of the modified phase retrieval algorithm is shown in Fig. S4[10]. Once the phase is synthesized in plane – 1, the complex amplitude can be propagated by any distance and the entire focal characteristics can be obtained.

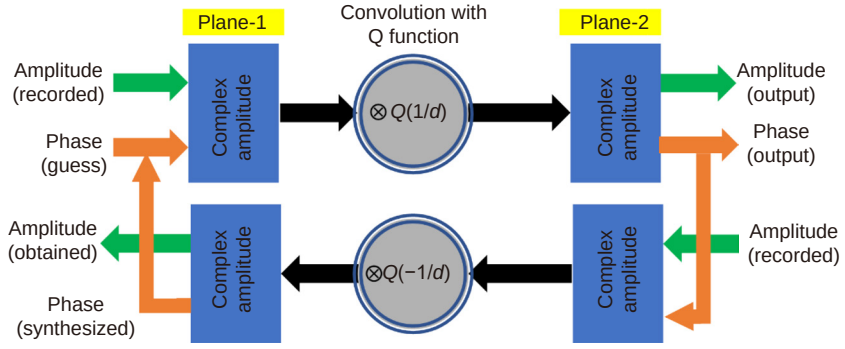

Fig. S4 | Modified phase retrieval algorithm. The field is propagated to the two planes back and forth by Fresnel propagation.

Section 5. Data structure conversion

The infrared microspectrometry unit (IRM) and the Fourier transform infrared (FTIR) spectrometer are linked by OPUS software of Bruker. The output from the OPUS software is saved as data point table format (*.dpt). The spectral images (64 × 64) for 765 channels obtained from the IRM FTIR system are structured into a matrix size of 765 × 4097. The spectral image data (64 × 64) is obtained from every row of the matrix 1 ∶ 4096 by rearrangement. The resulting cube data is of the structure (765 × 64 × 64). A single matrix is noisy and so multiple images (50 images) are averaged to obtain an image with a high signal to noise ratio. The image obtained from visible light is shown in Fig. S5(a). The im-

age of a single recording and average of 100 images are shown in Fig. S5(b) and S5(c) respectively. A MATLAB code is provided has been designed for the reformatting of data. The code is deposited online and can be downloaded here (10.5281/zenodo.5541384).

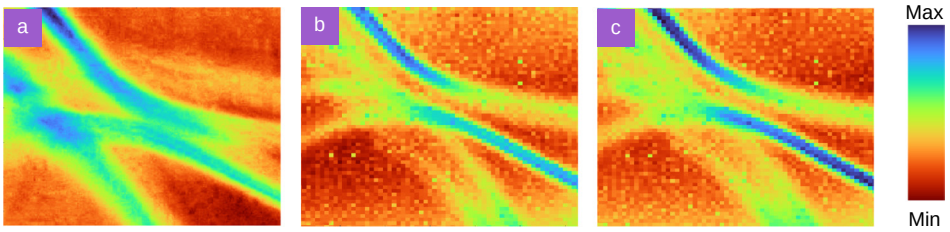

Fig. S5 | (**a**) Image obtained from visible light. (**b**) Single image and (**c**) averaged image (100 images) of the silk fibres recorded at the focal plane. Improvement in contrast can be noted in the averaged image.

References

1. Goodman JW. *Introduction to Fourier Optics* 3rd ed (Roberts & Company Publishers, Englewood, 2004).
2. Richardson WH. Bayesian-based iterative method of image restoration. *J Opt Soc Am* **62**, 55–59 (1972).
3. Lucy LB. An iterative technique for the rectification of observed distributions. *Astron J* **79**, 745 (1974).
4. Rai MR, Vijayakumar A, Rosen J. Non-linear adaptive three-dimensional imaging with interferenceless coded aperture correlation holography (I-COACH). *Opt Express* **26**, 18143–18154 (2018).
5. Horner JL, Gianino PD. Phase-only matched filtering. *Appl Opt* **23**, 812–816 (1984).
6. Lee K, Park Y. Exploiting the speckle-correlation scattering matrix for a compact reference-free holographic image sensor. *Nat Commun* **7**, 13359 (2016).
7. Antipa N, Kuo G, Heckel R, Mildenhall B, Bostan E et al. DiffuserCam: lensless single-exposure 3D imaging. *Optica* **5**, 1–9 (2018).
8. Anand V, Ng SH, Maksimovic J, Linklater D, Katkus T et al. Single shot multispectral multidimensional imaging using chaotic waves. *Sci Rep* **10**, 13902 (2020).
9. Kumar M, Vijayakumar A, Rosen J, Matoba O. Interferenceless coded aperture correlation holography with synthetic point spread holograms. *Appl Opt* **59**, 7321–7329 (2020).
10. Fienup JR. Phase retrieval algorithms: a comparison. *Appl Opt* **21**, 2758–2769 (1982).